J Mater Sci (2011) 46:4228–4235
DOI 10.1007/s10853-010-5239-0

IIB 2010

Shape and elastic state of nano-sized Ag precipitates in a Cu–Ag single crystal

Tomotaka Miyazawa · Toshiyuki Fujii · Susumu Onaka · Masaharu Kato

Received: 27 August 2010 / Accepted: 30 December 2010 / Published online: 20 January 2011

Abstract Using a single crystal of a Cu–6 mass% Ag alloy aged at 723 K for various times, nano-sized Ag precipitates in a Cu matrix were observed by conventional and ultra high-voltage transmission electron microscopes. The nano-sized Ag precipitates with a radius of about 5 nm had a nearly spherical shape. The shape change from the nearly spherical shape to the {111} octahedral shape occurred with increasing the size of the Ag precipitates to 11 nm. Elastic states of the Ag precipitates were evaluated by observing moiré fringes formed between the Ag precipitates and the Cu matrix. The origin of the shape change of the nano-sized Ag precipitates was discussed by considering the sum of elastic strain energy and interfacial energy.

Introduction

Cu and Ag form a typical eutectic system [1]. Cu and Ag phases of the Cu–Ag alloys have the interface of simple fcc–fcc lattice match [2–10]. The precipitation behavior of the alloys has been studied in many papers [2–12]. In the previous studies, formation of rod-like Ag precipitates in Cu-rich supersaturated solid solutions by discontinuous precipitation has been frequently examined. The discontinuous precipitation starts from grain boundaries in polycrystalline alloys [3–8, 11, 12].

Rod-like Ag precipitates have also been observed in grain interiors of the Cu–Ag alloys [9, 10]. In an aged single crystal of a Cu–5.7 mass% Ag alloy, Watanabe et al. [10] have observed the rod-like Ag precipitates with length of about 50–100 nm. They have also found that the cube-on-cube relationship exists between the Cu matrix and the Ag precipitates and that the rod-like Ag precipitates grow along the ⟨110⟩ direction of Cu and Ag [9, 10]. A large difference, about 13%, exists between the lattice constants of Cu and Ag [1]. This large misfit and its plastic accommodation at the Cu/Ag interface are important factors to understand the precipitation behavior in the Cu–Ag alloys. Considering the elastic states of the precipitates experimentally and theoretically, Watanabe et al. have presented a model of the accommodation of the misfit along the rod direction by prismatic dislocation loops surrounding the rod-like precipitates [10].

In an aged single crystal of the Cu–5.7 mass% Ag alloy, Monzen et al. [9] have observed nano-sized particulate Ag precipitates together with the rod-like precipitates. Such particulate precipitates in the alloy system with a large misfit are interesting research subjects to consider stable shapes of precipitates. However, as far as the authors know, neither the three-dimensional shape nor the elastic state of the nano-sized Ag precipitates has been discussed. In this study, we will investigate the nano-sized particulate Ag precipitates in a Cu–Ag single crystal. As will be shown later, the shape of the nano-sized Ag precipitates changes from spherical to octahedral during their growth. The purpose of this study is to understand the shape change of the nano-sized Ag precipitates by considering elastic strain energy and interfacial energy.

T. Miyazawa (✉) · S. Onaka · M. Kato
Department of Materials Science and Engineering, Tokyo Institute of Technology, 4259 Nagatsuta-cho, Midori-ku, Yokohama 226-8502, Japan
e-mail: miyazawa.t.ab@m.titech.ac.jp

T. Fujii
Department of Innovative and Engineered Materials, Tokyo Institute of Technology, 4259 Nagatsuta-cho, Midori-ku, Yokohama 226-8502, Japan

Experimental procedure

A Cu–6 mass% Ag alloy was prepared from 99.99% Cu and 99.99% Ag. A single crystal plate of the Cu–Ag alloy was grown in a graphite mold by the Bridgman method. The surface of the single crystal was parallel to (123). The specimens cut from the single crystal were solution-treated at 1103 K for 24 h, quenched into water and subsequently aged at 723 K for various times. Thin foils for transmission electron microscopy (TEM) were prepared from the aged specimens by mechanical and electrolytic polishing. TEM observations were carried out in a conventional TEM, JEOL JEM-2011 and an ultra high-voltage TEM (HVEM), HITACHI H-1250, operated at 200 and 1000 kV, respectively.

The shape of the particulate Ag precipitate was observed by TEM from three directions near [001], [101], and [111] of Cu. In addition, elastic strains of the Ag precipitates in the Cu matrix were evaluated by observing moiré fringes formed between the precipitates and the matrix [10]. For this purpose, it is necessary to exclude the effects of strain relaxation near the foil surface. Therefore, stereoscopic observation was made to select Ag precipitates embedded well into the thin foil [13, 14]. Figure 1 is an example of the result of the stereoscopic observation showing locations of the Ag precipitates in a cross-section of the Cu thin foil. The chosen Ag precipitates for the moiré fringe observation are those represented by the closed circles where the distance between the foil surface and the center of the precipitate is at least three times larger than the diameter of the precipitate.

Results

TEM observation of Ag precipitates

Particulate Ag precipitates were found in the Cu–6 mass% Ag single crystal aged at 723 K. All the particulate Ag precipitates observed in this study have a cube-on-cube orientation relationship with the Cu matrix. Figure 2a–c show bright-field (BF) images of the Ag precipitates taken from a direction near [001]. Figure 2d–f is the close-up views of the precipitates in Fig. 2a–c, respectively. Figure 2d shows a nearly spherical precipitate with a radius of about 5 nm observed in the specimen aged for 10 min at 723 K. It is found that when the precipitate radius is smaller than 5 nm, most of the precipitates have a nearly spherical shape. The shape was confirmed by observing the precipitates from various directions. With increasing the precipitate size, as shown in Fig. 2e and f, facet planes begin to be formed at the Ag/Cu interface. The facet planes become more noticeable for larger precipitates, though edges connecting the faceted planes are still round as shown in Fig. 2f.

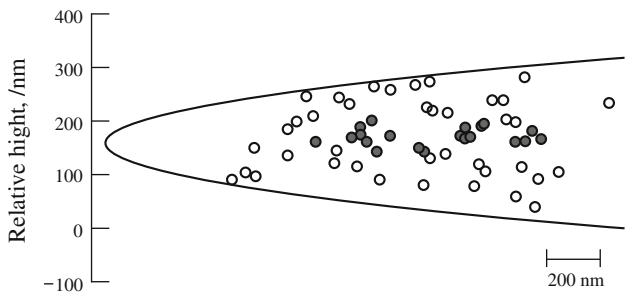

Fig. 1 An example of the result of stereoscopic observation showing locations of Ag precipitates in a cross-section of Cu thin foil. The Ag precipitates shown by *closed circles* embedded well into the thin foil were used to evaluate the elastic strains

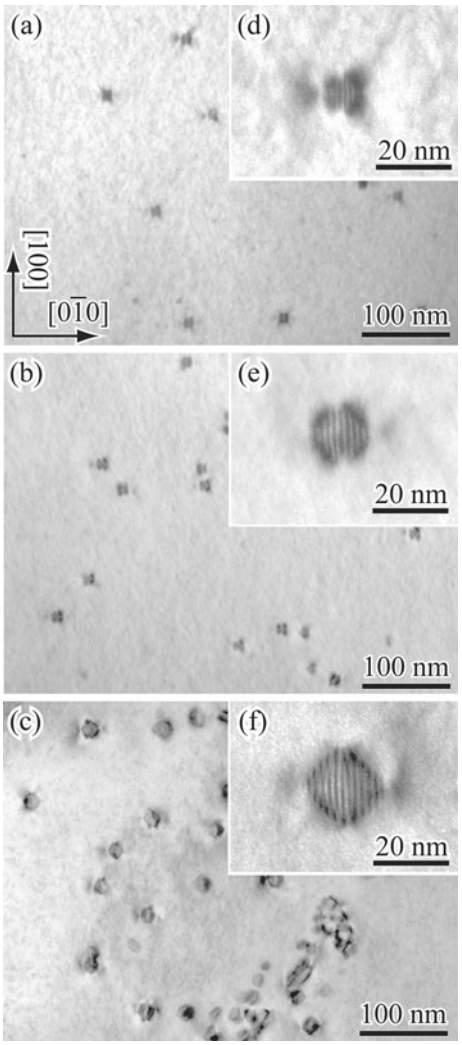

Fig. 2 Bright field images of Ag precipitates in a Cu matrix aged at 723 K for **a** 10 min, **b** 30 min, and **c** 60 min taken from a direction near [001] direction. *Insets* **d**, **e**, and **f** are the close-up views of Ag precipitates in **a**, **b**, and **c**, respectively

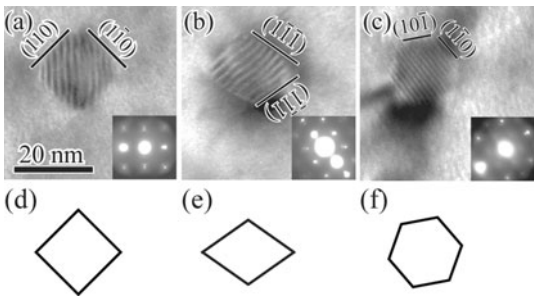

Fig. 3 An identical Ag precipitate in a Cu matrix observed from directions near **a** [001], **b** [101], and **c** [111]. This precipitate was observed in a specimen aged at 723 K for 60 min. Diffraction patterns corresponding to the micrographs are also shown in **a**–**c**. When we observe the {111} regular octahedron from the directions [001], [101], and [111], the corresponding projected shapes are *square*, *rhombus*, and *hexagon* as shown in **d** to **f**, respectively

A three-dimensional shape of the Ag precipitates with facet planes has been examined. Figure 3a–c shows the TEM images of an identical Ag precipitate observed from three different directions near [001], [101], and [111], respectively. When we observe a regular octahedron made of {111} planes from the directions [001], [101], and [111], the corresponding projected shapes are square, rhombus, and hexagon as shown in Fig. 3d–f, respectively. Comparison between the TEM images and projected shapes reveals that the shape of the Ag precipitate is close to a regular octahedron composed of {111}. However, the corners and edges of the Ag precipitate remain round even if the facet plane are well developed.

Superspherical approximation of the Ag precipitates

To treat geometrical and crystallographic characteristics of the observed shape change, the superspherical approximation [15–18] is appropriate. In Appendix A and Fig. 9, we have summarized geometrical characteristics of the supersphere of the {111} octahedral type expressing spherical, octahedral and their intermediate shapes. The shape parameter η $\left(1 \le \eta \le \sqrt{2}\right)$ giving the polyhedrality of the intermediate shape is also introduced in Appendix A, where the shapes with $\eta = 1$ and $\eta = \sqrt{2}$ show a spherical and the {111} octahedral shapes, respectively.

The shape of the Ag precipitate and its superspherical approximation are compared in Fig. 4. As shown in these figures, the superspherical approximation well reproduces the shape of the Ag precipitate. The shape parameter η given by Eq. 20 has a geometrical meaning written as

$$\eta = a_{\langle 100\rangle}/a_{\langle 110\rangle}, \tag{1}$$

where, as shown in Fig. 4b, $a_{\langle 110\rangle}$ is the diagonal radius along $\langle 110\rangle$ and $a_{\langle 100\rangle}$ the horizontal radius along $\langle 100\rangle$.

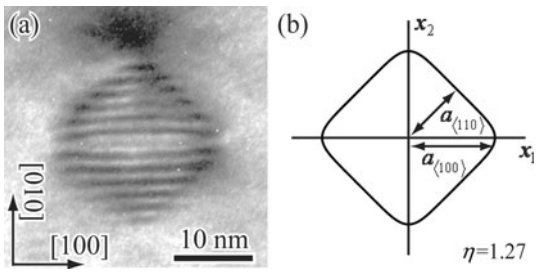

Fig. 4 Comparison of the shape of the Ag precipitate with that of the supersphere. **a** A close-up view of a Ag precipitate in a Cu matrix aged at 723 K for 60 min and **b** the [001] cross-section of the supersphere with $\eta = 1.27$

The volume V of the supersphere can be numerically calculated as a function of η and $a_{\langle 110\rangle}$ or $a_{\langle 100\rangle}$ [18]. The characteristic radius r given by

$$r = (3V/4\pi)^{1/3} \tag{2}$$

is used to show the size of the Ag precipitates. In Fig. 5, the relationship between r and η is shown for the Ag precipitates in specimens aged for various times. As can be seen, nearly spherical ($\eta \approx 1.0$) to nearly octahedral ($\eta \approx 1.3$) shape change occurs with increasing the precipitate size r from 5 to 11 nm. The solid line in Fig. 5 is a fitted curve just to show the trend of the shape change.

Moiré fringes in Ag precipitates

As shown in Figs. 2, 3, and 4, moiré fringes were observed between the Ag precipitates and the Cu matrix. Since the cube-on-cube relationship exists between the Ag precipitates and Cu matrix, the moiré fringes are the so-called parallel type caused by the difference of the lattice plane spacing between them. As shown in Fig. 4a, the moiré

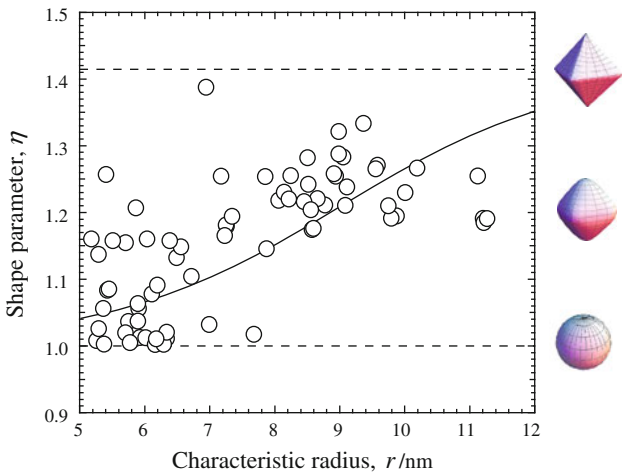

Fig. 5 The dependence of the shape parameter η as a function of the characteristic radius r of the Ag precipitates. The shapes corresponding to $\eta = 1$, $\eta = 1.2$, and $\eta = \sqrt{2}$ are also indicated

fringe spacing is not uniform in the Ag precipitate. The non-uniformity of the moiré fringe spacing comes from non-uniform elastic strains in a misfit precipitate with a non-ellipsoidal shape [19, 20]. We measured the average value D of the moiré fringe spacing for each Ag precipitate. Among the moiré fringe spacing D, the lattice plane spacing of Ag and Cu, d_{Ag} and d_{Cu}, we have the relation:

$$d_{Ag} = Dd_{Cu}/(D - d_{Cu}). \quad (3)$$

Here, the appropriate choice of d_{Ag} and d_{Cu} depends on the moiré fringe direction. That is, the {200} plane spacing should be used for Figs. 2, 3a, and 4, {111} for Fig. 3b, and {220} for Fig. 3c.

When the misfit due to the difference in the lattice constants are not accommodated at the Ag/Cu interface, elastic strains and stresses are created in and around the Ag precipitates. The lattice plane spacing of Ag in the elastically strained precipitate is, of course, different from the lattice plane spacing $d_{Ag}(0)$ calculated from $a_{Ag} = 0.4086$ nm without stresses [1]. Therefore, d_{Ag} in Eq. 3 is a function of elastic strain and will be written as $d_{Ag}(e)$ hereafter. On the other hand, since Cu foil with thickness is much larger than the size of the precipitate, we can safely ignore the elastic distortion of the Cu matrix and d_{Cu} in Eq. 3 can be regarded as $d_{Cu}(0)$ calculated from $a_{Cu} = 0.3615$ nm without stresses [1]. Then from Eq. 3, we can evaluate $d_{Ag}(e)$ in the Ag precipitates from D and $d_{Cu}(0)$ [10]. Using $d_{Ag}(e)$ thus evaluated, we can find the isotropic elastic strain e in the Ag precipitate:

$$e = \left[d_{Ag}(e) - d_{Ag}(0)\right]/d_{Ag}(0). \quad (4)$$

The moiré fringes of such embedded precipitates were observed from three different directions along [020], $[\bar{1}\bar{1}1]$, and $[\bar{2}20]$. Figure 6 shows the results of the observation along [020] where the values of the averaged elastic strain e in the Ag precipitate are plotted as a function of the characteristic radius r. The negative values of e means that the Ag precipitates are compressed by the Cu matrix. For the small nearly spherical precipitates with $r \approx 5$ nm, the elastic strain in the precipitates reaches about $-0.03 \sim -0.04$. On the other hand, for the large nearly octahedral precipitates with $r \approx 11$ nm, the elastic strain is about -0.005. The overall trend shown in Fig. 6 is the decrease in the magnitude of the elastic strain with increasing the precipitate size.

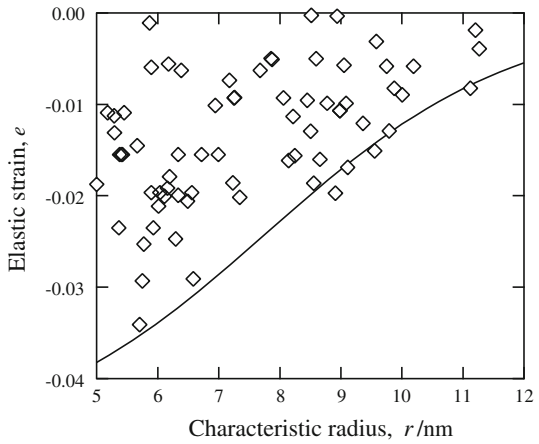

Fig. 6 The variation of the elastic strain e in the [020] direction as a function of characteristic radius r of the Ag precipitates. The *solid line* is a curve to fit the maximum absolute values of e as a function of r

Discussion

Elastic strains in the Ag precipitates

When difference between the lattice constants of Cu and Ag is only elastically accommodated, the resultant elastic strains can be evaluated by solving the inclusion problem of micromechanics [21]. Since the cube-on-cube orientation relationship exists between Ag and Cu, the eigenstrains or misfit strains ε^*_{ij} generated in the Ag precipitate are of a purely dilatational type written as

$$\varepsilon^*_{ij} = \delta_{ij}\varepsilon^*, \quad (5)$$

where δ_i is the Kronecker delta and ε^* is given by the lattice constants of Cu and Ag as

$$\varepsilon^* = \left(a_{Ag} - a_{Cu}\right)/a_{Cu} = 0.13. \quad (6)$$

As shown in Fig. 6, the absolute values of e are larger for smaller Ag precipitates with $r \approx 5$ nm and such small precipitates have a nearly spherical shape (Fig. 5). Therefore, assuming a spherical shape, we can calculate the elastic strains in the Ag precipitate using the inclusion problem of anisotropic elasticity [21]. For simplicity, the elastic moduli C_{ij} of Ag are assumed to be the same as those of Cu as $C_{11} = 16.84 \times 10^{10}$ Pa, $C_{12} = 12.14 \times 10^{10}$ Pa, $C_{44} = 7.54 \times 10^{10}$ Pa [22].

Using the procedure shown in Appendix B, we obtain isotropic elastic strain in the Ag precipitates as

$$e \approx -0.04. \quad (7)$$

Since e is uniform in a spherical precipitate, the brackets $\langle\rangle$ in Appendix B to show the averaged values are not needed in Eq. 7. The value of -0.04 is close to the maximum absolute magnitude of the measured elastic strain in the Ag precipitates with $r \approx 5$ nm, as shown in Fig. 6. This physically means that small Ag precipitates with $r \approx 5$ nm is almost coherent with the Cu matrix and the misfit is accommodated mainly by elastic distortion of the Ag precipitates and Cu matrix. On the other hand, the gradual decrease in the magnitude of e shown in Fig. 6 is explained by the occurrence of plastic relaxation (loss of

coherency) with generation of dislocations at the Cu/Ag interface [7, 10].

Energetics of shape change of Ag precipitates

To understand the shape change of the nano-sized Ag precipitates during growth shown in Fig. 5, let us discuss the energetics of the shape change. It is well known that the elastic strain energy and the interfacial energy play important roles in the shape change of precipitates [15, 23–25]. We consider the total energy G as a sum of the elastic strain energy E_{el} and the interfacial energy Γ for a material containing a precipitate:

$$G = E_{\mathrm{el}} + \Gamma. \tag{8}$$

In this equation, Γ means the chemical part of the interfacial energy caused by bonds between different kinds of atoms at the matrix/precipitate interface [26]. On the other hand, E_{el} is the mechanical energy due to elastic deformation in and around the precipitates. The change in the energy caused by the occurrence of plastic relaxation at the interface is also included in E_{el}.

Although the ellipsoidal inclusion problems cannot be applied to the case of superspherical inclusions, Onaka et al. have developed a method to evaluate the elastic states of superspherical inclusions [15, 16], as briefly described in Appendix B. According to the method, when a superspherical precipitate of the {111} octahedral type of volume V with $\varepsilon^*_{ij} = \delta_{ij}\varepsilon^*$ is embedded in matrix, E_{el} is written as (see Appendix B)

$$E_{\mathrm{el}} = \Phi(\eta) C_{44} (\varepsilon^*)^2 V, \tag{9}$$

where $\Phi(\eta)$ is the shape η dependent factor given by Eq. 27. Using the results shown in Fig. 10, the η dependence of $\Phi(\eta)$ is represented in Fig. 7. When the volume V and the eigenstrain ε^* are kept constant, the spherical shape is more stable than the octahedral shape when E_{el} determines the stable shape.

On the other hand, the interfacial energy Γ is generally written as

$$\Gamma = \int \gamma \mathrm{d}S, \tag{10}$$

where γ is the interfacial energy density, $\mathrm{d}S$ is the interface element on the precipitate and the integral is taken over the entire surface of a precipitate. Since evaluation of the anisotropy in γ is difficult, we will adopt the averaged interfacial energy density $\bar{\gamma}$ instead of γ to have

$$\Gamma = \bar{\gamma} S, \tag{11}$$

where S is the interface area of the precipitate. The orientation dependence of γ and the precipitate shape determine the averaged interfacial energy density $\bar{\gamma}$ for a certain precipitate. For the superspherical precipitate of the {111} octahedral type, using a dimensionless function g as a function of η shown in Fig. 8, the interface area S is written as

$$S = g(\eta) V^{2/3}. \tag{12}$$

As can be seen in Fig. 8, the interface area S under constant V rapidly increases with increasing η, when η is large.

From Eqs. 8, 9, 11, and 12, the total energy G as a sum of elastic and interfacial energies is rewritten as

$$G = \Phi(\eta) C_{44} (\varepsilon^*)^2 V + \bar{\gamma} g(\eta) V^{2/3}. \tag{13}$$

As shown in Fig. 5, the small Ag precipitates with $r \approx 5$ nm have a nearly spherical shape ($\eta \approx 1.0$). On the other hand, large Ag precipitates with $r \approx 11$ nm have a shape close to the {111} octahedron $\left(\eta = \sqrt{2}\right)$. From these experimental observations, the following inequalities can be obtained on the total energy G.

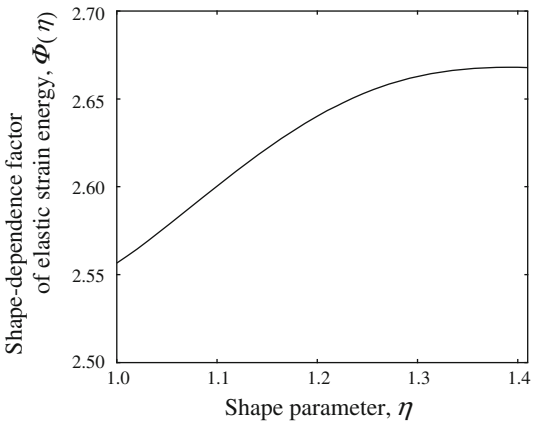

Fig. 7 The η dependence of shape-dependence factor $\Phi(\eta)$ of the elastic strain energy for a superspherical precipitate of the {111} type Cu with $A_{\mathrm{r}} = 3.2$ and $v_{100} = 0.42$

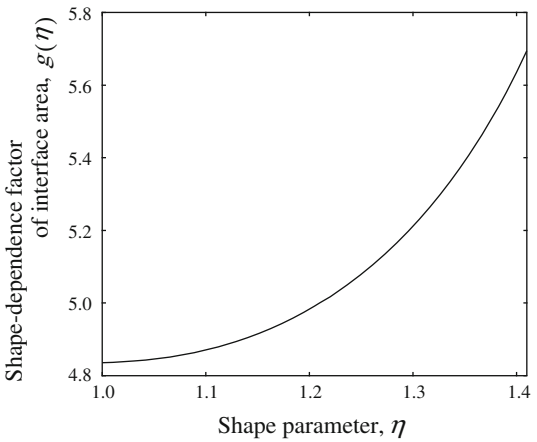

Fig. 8 The η dependence of shape-dependence factor $g(\eta)$ of the interface area for a superspherical precipitate of the {111} type

$$G(r = 5\,\text{nm},\ \eta = 1) < G\left(r = 5\,\text{nm},\ \eta = \sqrt{2}\right) \tag{14}$$

and

$$G(r = 11\,\text{nm},\ \eta = 1) > G\left(r = 11\,\text{nm},\ \eta = \sqrt{2}\right). \tag{15}$$

The η dependences of $\Phi(\eta)$ and $g(\eta)$ are shown in Figs. 7 and 8. Since all the parameters and constants except $\bar{\gamma}$ are now known, we can numerically evaluate η-dependent G in Eq. 13 as a function of $\bar{\gamma}$. Then, from inequalities 14 and 15, the upper and lower bounds of $\bar{\gamma}_{\text{sphere}}/\gamma_{111}$, where $\bar{\gamma}_{\text{sphere}} \equiv \bar{\gamma}(\eta = 1)$ and $\gamma_{111} \equiv \bar{\gamma}\left(\eta = \sqrt{2}\right)$, can be obtained by assuming that $\bar{\gamma}$ is independent of r as

$$1.34 < \bar{\gamma}_{\text{sphere}}/\gamma_{111} < 1.75. \tag{16}$$

As mentioned previously, the decrease in the absolute magnitude of e with increase in r (Fig. 6) physically means more occurrence of plastic accommodation, i.e., Ag precipitates gradually lose coherency as they become larger. From the micromechanics point of view, this again means that the misfit strain ε^* becomes smaller as precipitates grow [27]. Therefore, to obtain inequality 16, the values of r-dependent ε^* were back-calculated using the $r - e$ relationship shown by the solid curve in Fig. 6.

For the Cu/Ag {111} interface, $\gamma_{111} = 0.23\,\text{J/m}^2$ was reported by Bacher et al. [28]. On the other hand, $\bar{\gamma}_{\text{sphere}}$ is the averaged interfacial energy density for a spherical precipitate. For interfaces composed of cube-on-cube fcc crystals, it is generally accepted that γ_{111} has the smallest energy density [29]. Considering the degree of the magnitude of the anisotropy of γ [29], the bounds shown by inequality 16 are quite reasonable.

Since $E_{\text{el}} \propto r^3$ and $\Gamma \propto r^2$, it is generally understood that Γ controls the shape of smaller precipitates and E_{el} controls the shape of larger precipitates. If so, one may think that the smaller precipitates should have been an {111} octahedron (with the smallest Γ) and the larger precipitates should have been a sphere (with the smallest E_{el}), although the present results are just opposite. This apparent discrepancy arises when the r-dependent behavior of ε^* is overlooked. In reality, the loss of coherency in larger precipitates leads to the decrease in ε^*, as mentioned above. Therefore, the contribution of elastic strain energy is larger for smaller precipitates and smaller for larger precipitates. This is the reason why the shape change from spherical to octahedral takes place during the growth of the Ag precipitate.

Conclusions

Using a single crystal of a Cu–6 mass% Ag alloy aged at 723 K for various times, nano-sized Ag precipitates in a Cu matrix were observed by TEM. The following conclusions have been obtained.

(1) The nano-sized Ag precipitates with a radius of about 5 nm had a nearly spherical shape. The change from the nearly spherical shape to a {111} octahedral shape occurred with increasing the size of the Ag precipitates to 11 nm.
(2) The superspherical approximation well reproduces the shapes of the Ag precipitates between a sphere and the {111} octahedron.
(3) The absolute magnitude of the elastic strains in the Ag precipitates decreased with increasing the size of the precipitates. The maximum magnitude of the elastic strain in the Ag precipitates with $r \approx 5$ nm is explained by the elastic accommodation of the lattice misfit between Ag and Cu.
(4) The origin of the shape change of the nano-sized Ag precipitates is explained by considering the sum of elastic strain energy and interfacial energy.

Acknowledgements This research was supported by a Grand-in-Aid for Scientific Research C (19560690) by Japan Society for Promotion of Science and by the "Nanotechnology Network Project" of the Ministry of Education, Culture, Sports, Science, and Technology (MEXT), Japan. We are grateful to Professor Emeritus Akikazu Sato of Tokyo Institute of Technology for helping the observations and fruitful comments. We are also grateful to Professors Ryoichi Monzen and Chihiro Watanabe of Kanazawa University for the provision of Cu–Ag alloys.

Appendix

A: Supersphere of the {111} octahedral type

The Co–Cr precipitates in a Cu matrix and the γ' precipitates in Ni-base heat-resistant alloys have cuboidal shapes with round corners [15]. To approximate such precipitate shapes between a sphere and the cube, the supersphere of a cubic (hexahedral) type was considered [15]. The supersphere of the cubic type has been extended to other types of superspheres [16–18]. On the $x - y - z$ orthogonal coordinate system, a supersphere of an octahedral type is written as [16–18]

$$\begin{aligned}&|(x+y+z)/R|^p + |(x-y+z)/R|^p + |(x+y-z)/R|^p \\ &\quad + |(-x+y+z)/R|^p = 1,\end{aligned} \tag{17}$$

where $p(p \geq 2)$ is a shape parameter and $R(R > 0)$ is a size parameter. When $p = 2$, Eq. 17 reduces to

$$4\left(x^2/R^2 + y^2/R^2 + z^2/R^2\right) = 1, \tag{18}$$

a sphere with a radius of $R/2$. On the other hand, when $p \to \infty$, Eq. 17 describes the regular octahedron composed of the four sets of parallel planes:

$$x + y + z = \pm R,\ x - y + z = \pm R,\ x + y - z = \pm R,$$
$$\text{and } -x + y + z = \pm R. \tag{19}$$

When the x, y, and z axes of the coordinate system are, respectively, parallel to the [100], [010], and [001] directions of a cubic crystal, Eq. 17 with an appropriate value of $p (p \geq 2)$ describes an intermediate shape between an {111} octahedron and a sphere.

Instead of p, η given by

$$\eta = \sqrt{2} \cdot 2^{(-1/p)}$$
$$\left(\eta = 1 \text{ when } p = 2, \text{ and } \eta = \sqrt{2} \text{ when } p \to \infty\right) \tag{20}$$

is a more convenient shape parameter to handle. A geometrical meaning of the shape parameter η for the supersphere of the octahedral type is shown in Fig. 4. The three-dimensional shapes and projections of the supersphere of an octahedron type are represented in Fig. 9 for various values of η.

B: Inclusion problem for the superspherical inclusion of the {111} octahedral type

To examine elastic states of materials containing precipitates with misfit strains ε^*_{ij}, the Eshelby method for ellipsoidal inclusions is a very powerful tool [30, 31]. It is well known that if uniform ε^*_{ij} exists in an ellipsoidal inclusion, strains and stresses in the inclusion also become uniform. For a superspherical inclusion, on the other hand, the uniformity of strains and stresses no more holds even if ε^*_{ij} is uniform in the inclusion. However, the Eshelby method can be extended to non-ellipsoidal inclusions if we consider averaged values in the inclusions. Consider an infinitely extended material with homogeneous elastic moduli C_{ijkl}. When an inclusion Ω with C_{ijkl} having uniform eigenstrains ε^*_{ij} is embedded in the material, the averaged total strains $\langle \varepsilon_{ij} \rangle$ in Ω are written as

$$\langle \varepsilon_{ij} \rangle = \langle S_{ijkl} \rangle \varepsilon^*_{kl}, \tag{21}$$

where $\langle S_{ijkl} \rangle$ are the averaged Eshelby tensors [32, 33].

Then, the averaged elastic strains $\langle e_{ij} \rangle$ in Ω is given by

$$\langle e_{ij} \rangle = \langle \varepsilon_{ij} \rangle - \varepsilon^*_{ij} = \langle S_{ijkl} \rangle \varepsilon^*_{kl} - \varepsilon^*_{ij}. \tag{22}$$

The elastic strain energy E_{el} due to Ω with ε^*_{ij} is written as [15, 16]

$$E_{\text{el}} = -\frac{1}{2}\left\{C_{ijkl}\left(\langle S_{klmn} \rangle \varepsilon^*_{mn} - \varepsilon^*_{kl}\right)\right\}\varepsilon^*_{ij} V, \tag{23}$$

where V is the volume of Ω.

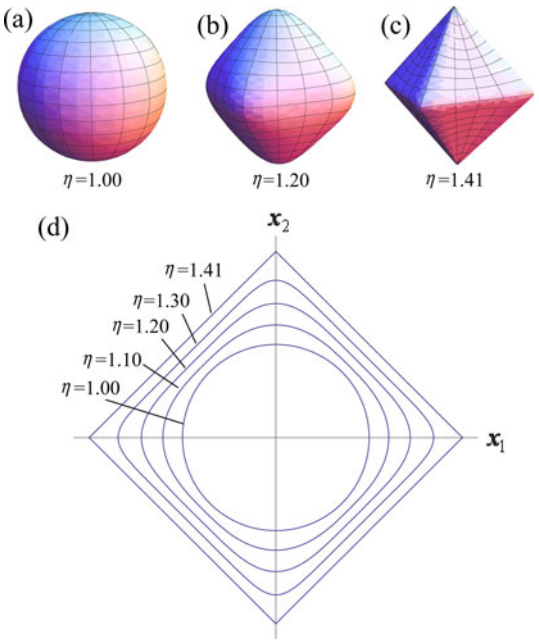

Fig. 9 The three-dimensional shapes of a supersphere of the {111} octahedral type with **a** $\eta = 1.00$, **b** $\eta = 1.20$, and **c** $\eta = 1.41$. **d** The {001} cross-sections of the supersphere for various values of η

When the superspherical inclusion of the {111} octahedral type has purely dilatational eigenstrains $\varepsilon^*_{ij} = \delta_{ij}\varepsilon^*$, the averaged elastic strains $\langle e_{ij} \rangle$ given by Eq. 22 is rewritten as

$$\langle e_{ij} \rangle = \delta_{ij} \langle e \rangle, \tag{24}$$

where

$$\langle e \rangle = (\langle S_{1111} \rangle + 2\langle S_{1122} \rangle - 1)\varepsilon^*. \tag{25}$$

On the other hand, the elastic strain energy E_{el} given by Eq. 23 is rewritten as [15, 16]

$$E_{\text{el}} = \Phi(\eta) C_{44} (\varepsilon^*)^2 V, \tag{26}$$

where

$$\Phi(\eta) = \frac{3(1 + \nu_{100})}{A_{\text{r}}(1 - 2\nu_{100})}(1 - \langle S_{1111} \rangle - 2\langle S_{1122} \rangle). \tag{27}$$

Here, $\Phi(\eta)$ represents the shape η dependence of E_{el}, and C_{44} is one of the elastic moduli of a cubic material in the Voigt notation, A_{r} the anisotropy ratio of the elastic moduli and ν_{100} the Poisson ratio for $\langle 100 \rangle$ extension. The elastic moduli for Cu can be fully expressed by a set of moduli: $C_{44} = 7.54 \times 10^{10}$ Pa, $A_{\text{r}} = 3.2$, and $\nu_{100} = 0.42$ [15, 22]. The components of $\langle S_{ijkl} \rangle$ for superspherical inclusions of the {111} octahedral type can be calculated using the method shown in [15]. The shape parameter η dependence of $\langle S_{1111} \rangle$ and $\langle S_{1122} \rangle$ for Cu are shown in Fig. 10.

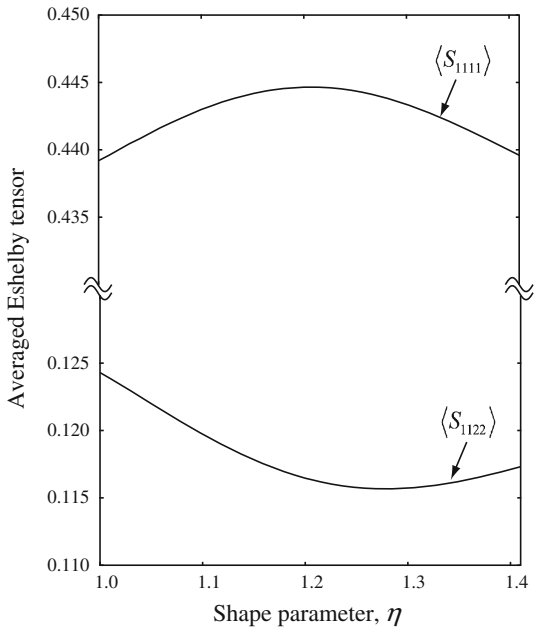

Fig. 10 The η dependence of $\langle S_{1111} \rangle$ and $\langle S_{1122} \rangle$ for the superspherical inclusions of the {111} type in Cu with anisotropic elastic moduli with $A_r = 3.2$ and $\nu_{100} = 0.42$

References

1. Massalski TB, Subramanian PR, Okamoto H, Kacprzak L (1990) Binary alloy phase diagrams, 2nd edn, vols 1–3. ASM International, Materials Park, OH
2. Räty R, Miekk-oja HM (1968) Philos Mag 18:1105
3. Wirth R, Gleiter H (1981) Acta Metall 29:1825
4. Gust W, Beuers J, Steffen J, Stiltz S, Predel B (1986) Acta Metall 34:1671
5. Manna I, Pabi SK (1990) J Mater Sci Lett 9:1226
6. Spaic S, Pristavec M (1997) Z Metallk 88:925
7. Rao G, Zhang D, Wynblatt P (1993) Scripta Metall Mater 28:459
8. Gupta SP (1998) Can Metall Q 37:141
9. Monzen R, Murase K, Nagayoshi H, Watanabe C (2004) Philos Mag Lett 84:349
10. Watanabe C, Monzen R, Nagayoshi H, Onaka S (2006) Philos Mag Lett 86:65
11. Leo W (1967) Z Metallk 58:456
12. Kainuma N, Watanabe R (1969) J Japan Inst Metals 33:198
13. Niwa T, Ikematsu Y, Taniyama A, Shindo D (2003) J Japan Inst Metals 67:93
14. Kiritani M (1981) Denshi Kenbikyo 16:71
15. Onaka S, Kobayashi N, Fujii T, Kato M (2003) Mater Sci Eng A A347:42
16. Onaka S, Fujii T, Kato M (2007) Acta Mater 55:669
17. Onaks S (2006) Philos Mag Lett 86:175
18. Onaka S (2008) J Mater Sci 43:2680. doi:10.1007/s10853-007-2439-3
19. Markenscoff X (1998) J Mech Phys Solids 46:2297
20. Zou WN, He QC, Huang MJ, Zheng QS (2010) J Mech Phys Solids 58:346
21. Mura T (1987) Micromechanics of defects in solids, 2nd edn. Martinun Nijhoff, Dordrecht
22. Hirth JP, Lothe J (1992) Theory of dislocations, 2nd edn. Kringer, Malabar
23. Fujii T, Tamura T, Onaka S, Kato M (2002) Microsc Microanal 8:1434
24. Watanabe D, Watanabe C, Monzen R (2008) Metall Mater Trans A 39:725
25. Watanabe D, Watanabe C, Monzen R (2009) Acta Mater 57:1899
26. Turnbull D (1955) Impurities and imperfections. ASM, Metals Park, Ohio, p 121
27. Kato M, Fujii T, Onaka S (1996) Mater Sci Eng A 211:95
28. Bacher P, Wynblatt P, Foiles SM (1991) Acta Metall Mater 39:319
29. Lee YW, Aaronson HI (1980) Acta Metall 28:539
30. Eshelby JD (1957) Proc R Soc A 241:376
31. Eshelby JD (1959) Proc R Soc A 252:561
32. Onaka S (2001) Philos Mag Lett 81:265
33. Onaka S (2000) Philos Mag Lett 80:367